Estimation of Coastal Floridan Aquifer Properties from Spectral Analysis of Ocean Tidal Linear Systems Forcing

October 31 2006

Joseph Park[1], Emily Richardson[2]

1. Hydrologic & Environmental Systems Modeling (7540)
2. Resource Evaluation/Sub-Regional Modeling (4330)

South Florida Water Management District
West Palm Beach, Florida, USA

Abstract

Spectral analysis techniques are adapted and applied to hydrologic, oceanographic, and meteorologic data to characterize Floridan Aquifer transport metrics along the southeast coast of Florida. Three hydrologic analytical models are applied based on ocean tidal forcing to aquifer well response. None of the three models produced results consistent with the sparse APT data. It is inferred that three models do not provide an adequate representation of the geophysical interface between the Floridan Aquifer and Atlantic Ocean. It is shown that spectral coherence and linear systems modeling can be used to isolate barometric forcing from ocean tidal forcing on aquifer well response. A method of estimating barometric efficiency based on spectral analysis is proposed, but results are not useful due to nonlinear coupling of barometric pressure into the well data. It is also shown that certain frequencies of the Floridan well data are dominated by tidal forcing, this dominance can invalidate assumptions inherent in Clark's method for estimation of barometric efficiency on short timescales. Further, it verifies that tidal forcing should be included in hydrological models applied to the coastal Floridan Aquifer.

Contents

List of Figures

List of Tables

1 Introduction

Over the last decade, use of the Floridan Aquifer System (FAS) as a water source within the SFWMD has been growing, and is anticipated to expand even faster in the decade to come. Improvements in reverse osmosis (RO), aquifer storage and recovery (ASR) technologies, and increasing limitations on traditional water sources have enhanced the appeal of FAS use. It is not, however, without risk. On the lower east coast (LEC) Palm Beach, Broward and Miami-Dade Counties, the depth of the FAS, and it's brackish quality make the investment required to develop it as a viable source significantly greater than for the shallow aquifers traditionally used in these areas. Because it has been lightly developed, the hydrogeology of the FAS and how it will respond to increasing stresses are poorly understood.

Preliminary efforts to model the system have identified particular weaknesses affecting our understanding on the southeast coast: lack of monitor data to support model boundaries in the interior of the state, uncertainties in the location and mechanism of off-shore boundary conditions, lack of time-series data in the deeper hydrogeologic units, and increasing scarcity of aquifer hydraulic parameters with depth. Time and funding limitations restrict our abilities to fill all of these data gaps through drilling and testing of additional exploratory wells into the Floridan, prompting the need for alternative means of data acquisition.

This paper explores the use of spectral analysis and linear systems modeling to characterize the aquifer based on its response to ocean tidal forcing. Three objectives are pursued:

1. Calculation of aquifer hydraulic properties in the absence of traditional field testing.
2. Provide independent information on off-shore boundary conditions to guide model calibration.
3. Evaluate the application of spectral analysis methods, routinely employed in signal processing applications, to hydrogeologic investigation.

This is achieved through analysis of ocean tidal forcing on aquifer well levels from which coupling coefficients are estimated. The coefficients quantify relative power amplitude of discrete spectral components between the ocean tidal and well stages, and are a fundamental parameter for estimation of aquifer transport properties.

If the ocean tidal forcing and aquifer response constituted a single-input single-output (SISO) linear system, analysis could proceed with SISO

cross-spectral techniques applied to the two data sets. However, both the ocean tidal behavior and the aquifer well responses are dependent upon atmospheric pressure forcing. A conceptual illustration of this coupled system is shown in figure 1.

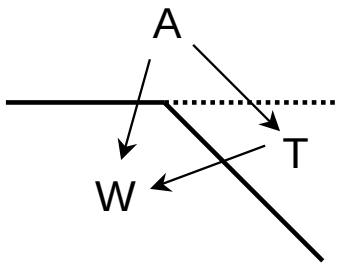

Figure 1: Conceptualization of coupled atmospheric pressure (A), ocean tidal (T) and aquifer well stage (W).

As a result of the coupled nature of these systems, care must be exercised in isolation of geophysical forcings between them. Conventional approaches for separation of atmospheric pressure forcings from the ocean tidal and aquifer response rely on timeseries filtering and detrending to account for atmospheric influence. The authors have taken a different approach to this issue by using spectral coherence and transfer functions to identify atmospheric coupling components. Once identified, the effected spectral components are excluded from the ocean to aquifer coupling analysis. An advantage of this approach is that the geophysical data are used 'as-is', there is no detrending, filtering or data preprocessing. Not only can this result in a reduction of analysis overhead, it also avoids a potential source of error and bias introduction.

The analysis is performed on FAS monitor well data from two sites, one in Palm Beach and the other in Broward County. Atmospheric and ocean tidal data were also extracted from two sites in Palm Beach and Broward County. Figure 2 illustrates location of the wells and atmospheric/oceanic monitoring stations.

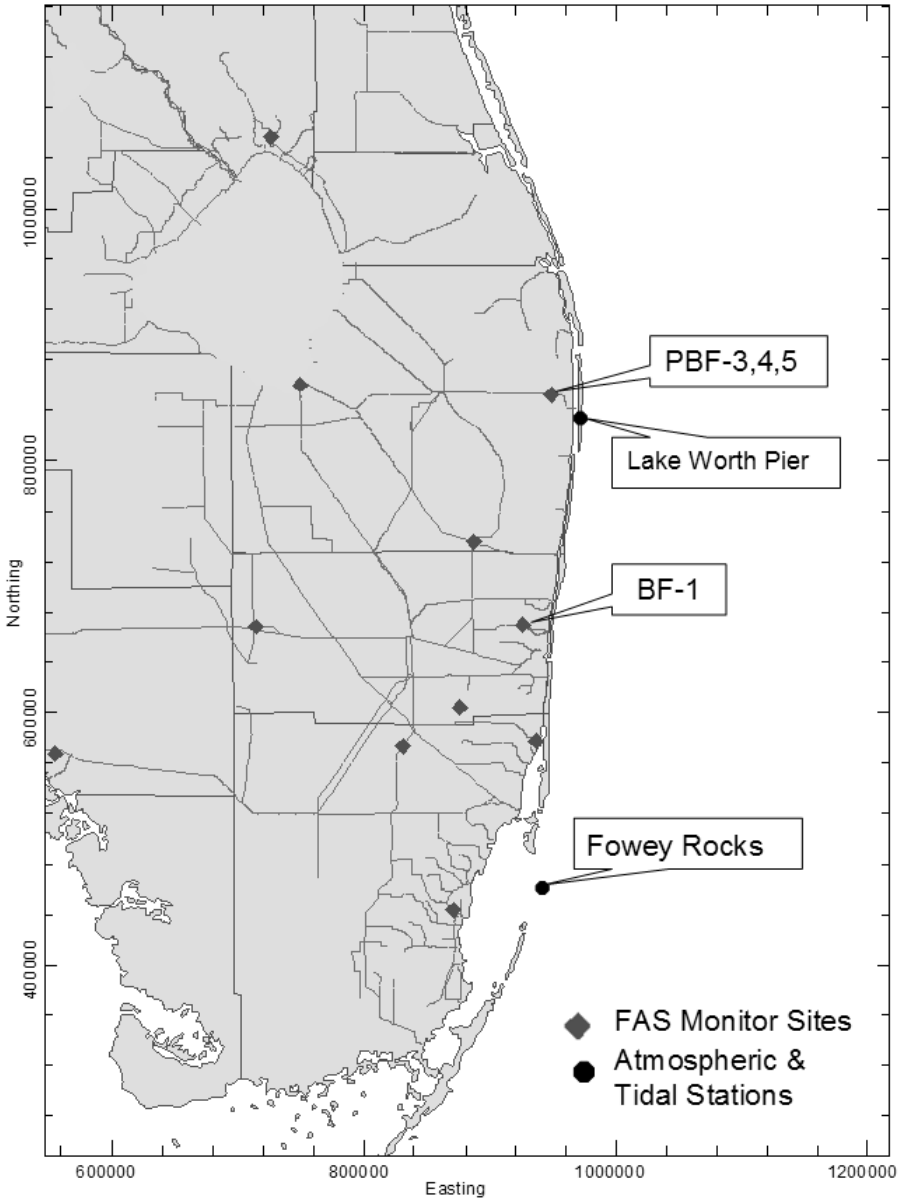

Figure 2: Location of Floridan Aquifer monitor wells, and the meteorological stations in Palm Beach, and Broward Counties used in the estimation of aquifer transport.

2 Meteorological, Oceanographic & Hydrological Data

Estimation of coupling coefficients between the ocean tidal forcing and aquifer well response is dependent on three coupled data sets:

1. Atmospheric Pressure (A)
2. Floridan Aquifer Well Stage (W)
3. Ocean Tidal Stage (T)

Data extraction and preparation for each of these components is described below. The period of record for this analysis encompassed January 1st, 2002 through December 31st, 2004. Notable climatic events during this period included Hurricane Frances (September 5th 2004) and Hurricane Jeanne (September 25, 2004).

2.1 Atmospheric Pressure and Tidal Data

Atmospheric pressure data was extracted from NOAA National Data Buoy Center (NDBC) Coastal Marine Automated Network (C-MAN) stations at Lake Worth Pier [NOAA LKWF1, 2006], and Fowey Rocks [NOAA FWYF1, 2006] Florida. Ocean tidal data was also extracted from the C-MAN station at Lake Worth Pier. The data sampling interval is one hour. Shortly after the passage of Hurricane Jeanne, the C-MAN station at Lake Worth Pier failed, subsequently, the ocean tidal and barometric pressure data from Lake Worth ended on October 5, 2004.

Figure 3 plots the hourly atmospheric pressure and ocean tidal data over the period of record. Even though the Lake Worth Pier and Fowey Rocks stations are separated by a distance of 113.9 km (70.8 miles) there is high correlation between the two timeseries ($r^2_{xy} = 0.96$).

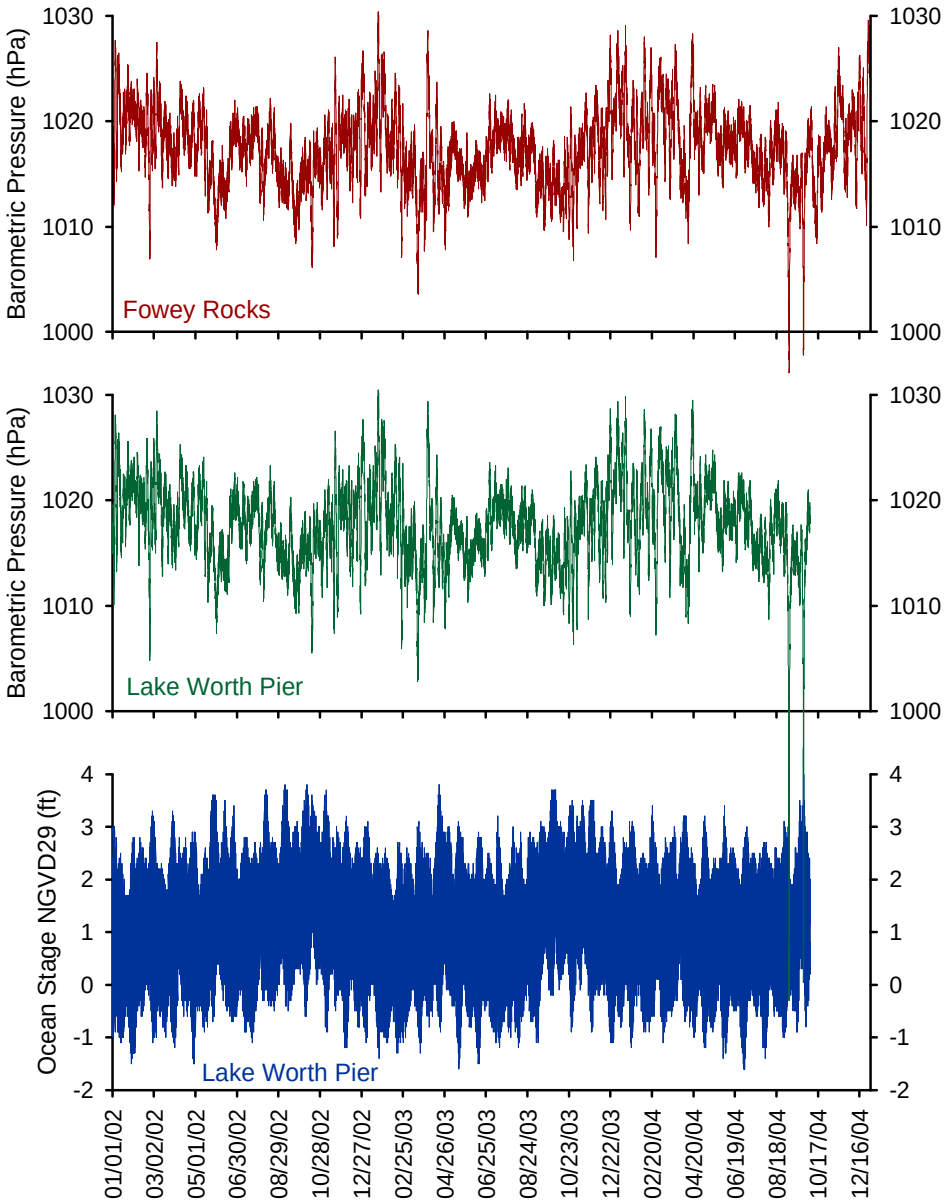

Figure 3: Barometric pressure and ocean water level over period of record.

A short period view of the barometric and ocean water level measurements are shown in figure 4. High correlation between the barometric pressure data is evident, as well as the semi-diurnal ocean water level fluctuations driven by tidal forcing. The barometric pressure data indicate the passage of a low pressure boundary, from which one can observe a concomitant increase in the average level of the ocean water levels. Closer inspection reveals evidence of the inverse barometer effect [Apel, 1987] which predicts from simple hydrostatics that the change in ocean surface elevation (in centimeters) is numerically the same as, but opposite in sign to the change in atmospheric pressure (in millibars). For example, the change in pressure at Lake Worth Pier from the minima on November 3rd to the same time period on the next day is approximately 8 hPa (mb). The reduction in water level from the corresponding high tide maxima are roughly 8 cm (0.26 ft).

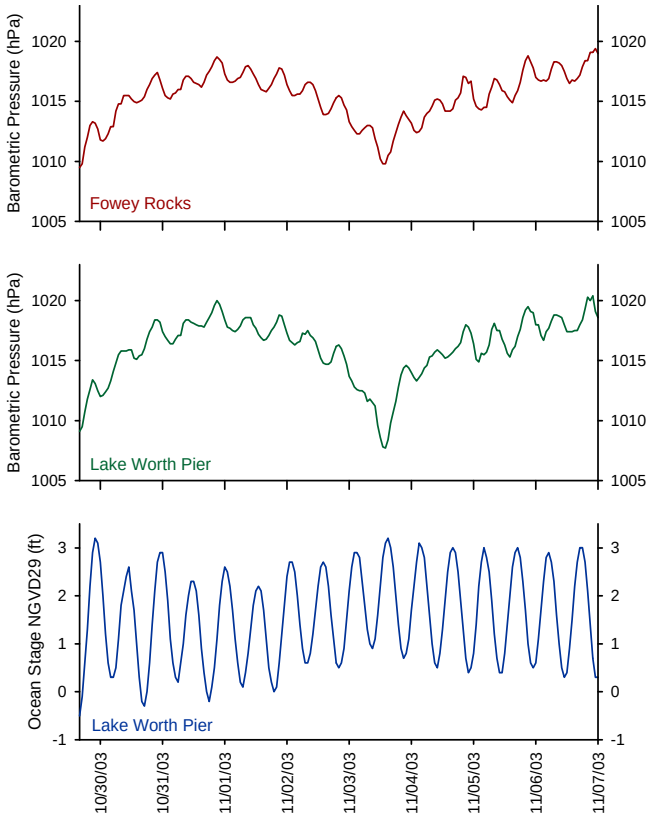

Figure 4: Barometric pressure and ocean water level over a short period.

2.2 Groundwater Data

Native groundwater levels for the period from January, 2002 to December, 2004, from two SFWMD monitor sites, representing three distinct permeable zones within the Floridan Aquifer System, were compiled for this project. Figure 5 illustrates the construction of wells utilized, and the hydrogeologic units they represent. The sites were chosen for: their proximity to the coast, continuity of record, and the availability of field test data with which to support or critique the tidal forcing analysis.

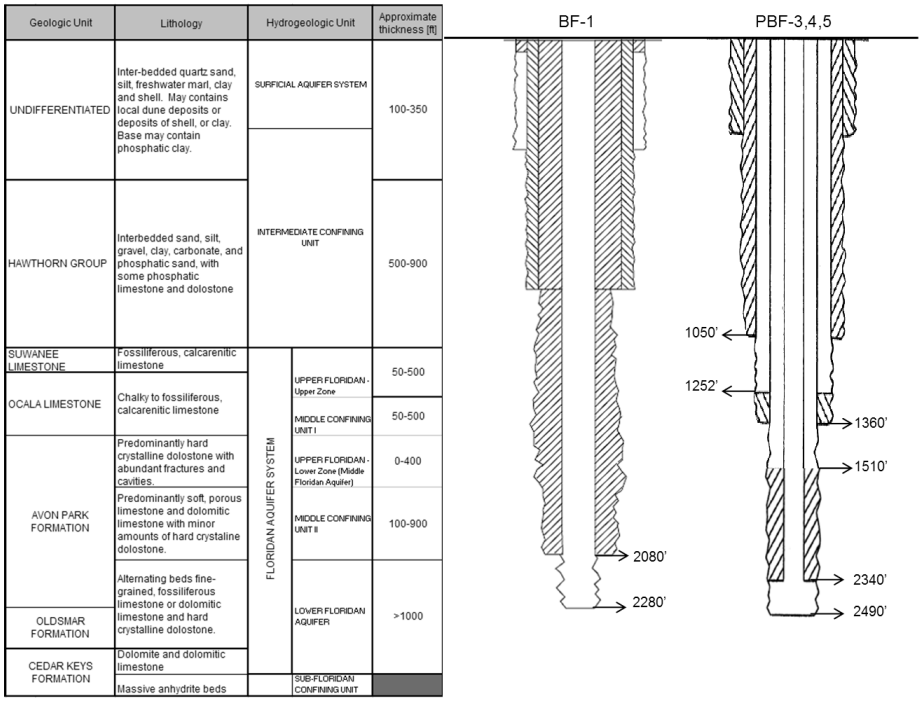

Figure 5: Hydrogeologic formations of the Floridan Aquifer monitor wells, and well construction details.

The Palm Beach County site is a tri-zone well monitoring the upper (PBF-3), middle (PBF-4) and lower (PBF-5) Floridan Aquifers. Heads in PBF-3 and PBF-4 are under artesian pressure, and track one another with generally less than a foot of difference, indicating some hydraulic connection. The water is also similar in chemical composition, with typical salinities around 4,000 mg/l total dissolved solids (TDS). Heads in PBF-5 are non-artesian, and salinity approaches that of seawater (31,000 mg/l TDS), indicating significant confinement between the middle and lower Floridan at this site. Aquifer performance testing on the upper and middle Floridan yielded transmissivity estimates of 34,300 ft^2/day and 198,500 ft^2/day respectively. No performance testing is available on the lower Floridan Aquifer at this location. A complete description of the construction and testing of this site is provided in [Lukasiewicz, 2001].

In Broward County, data from the lower Floridan monitor well (BF-1) at the District's Oakland Park test site was utilized. Monitor data from the upper and middle Floridan aquifers was available at this site as well, but was excluded from the study because it appeared to be strongly influenced by pumping stresses which could mask the tidal signal. Heads in the lower Floridan at this site are also non-artesian, generally several feet below land surface, and chemistry is similar to PBF-5 (TDS 32,000 mg/l). No aquifer performance test data is available for BF-1, but packer testing of was performed on two isolated intervals (2078-2120 and 2120-2142) within the monitored zone. Results of the packer testing yielded specific capacity values of 0.07 (gal/min/ft) in the upper interval, and 550 (gal/min/ft) in the lower interval. Based on those specific capacities, rule of thumb convention would yield transmissivity value estimates from 19 to 147,000 ft^2/day. These are not high confidence estimates, but they are good indicators of extreme heterogeneity within the aquifer. A complete description of the construction and testing of this site is provided in [Lukasiewicz, 2003].

Plots of the Floridan Aquifer well data are presented in figure 6.

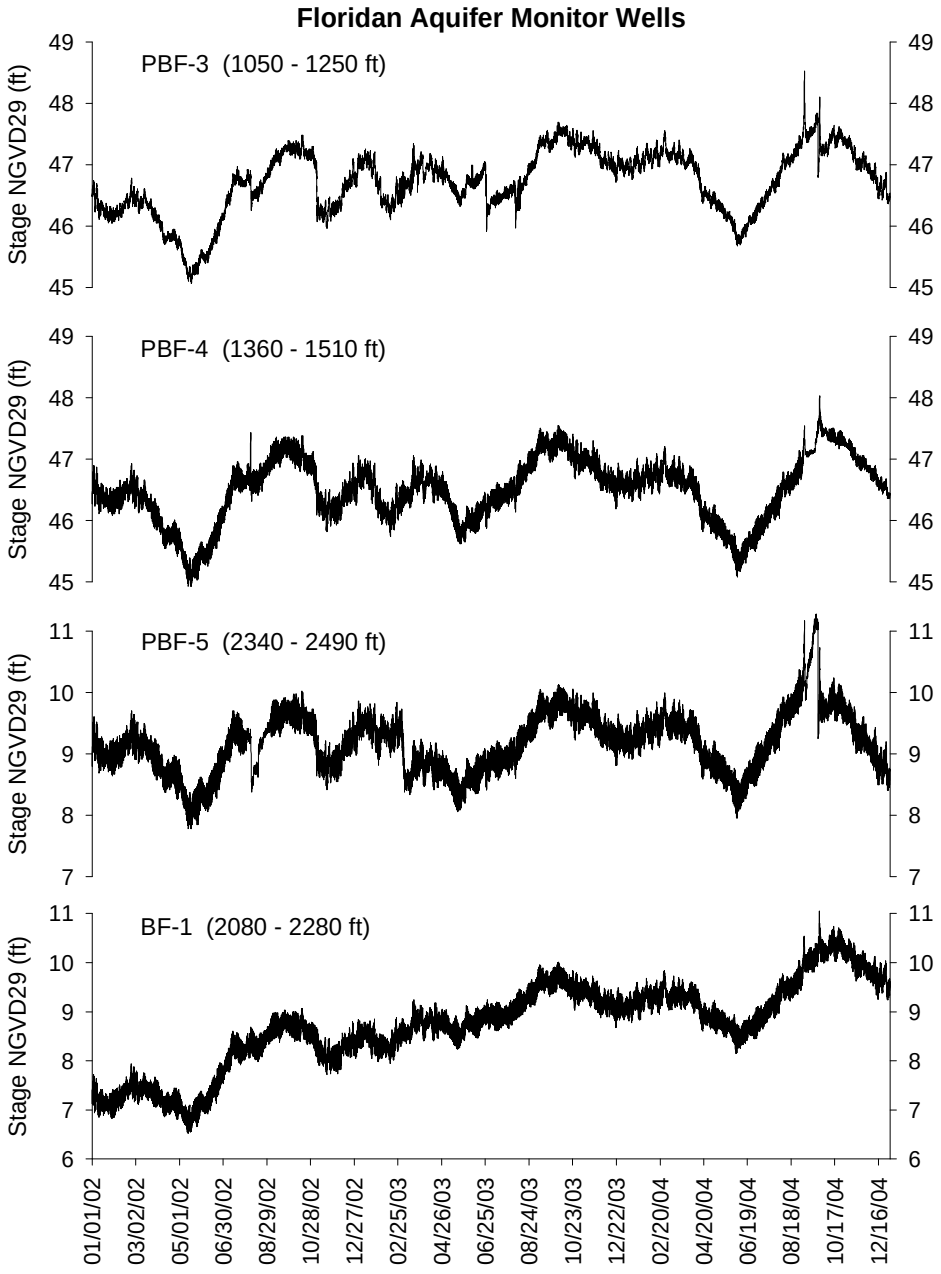

Figure 6: Floridan Aquifer well stage over period of record.

2.2.1 Data Extrapolation

Aquifer well timeseries inevitably exhibit data gaps when collected over long periods, usually associated with instrumentation maintenance or reliability. One potential resolution to this issue is to limit the data analysis to sections of data which were continuously sampled, however, loss of ensemble averaging would result in larger spectral estimation errors. Therefore, missing data was identified and extrapolated by one of two methods: linear interpolation, or reconstruction from correlated data with residual bias terms. Table 1 lists the extent of missing data for each of the aquifer well timeseries.

	PBF-3	PBF-4	PBF-5	BF-1
Total Points	26,304	26,304	26,304	26,304
Data Points	25,481	25,065	24,775	26,299
Data Present	96.87%	95.29%	94.19%	99.98%
Data Missing	3.13%	4.71%	5.81%	0.02%

Table 1: Measured well data availability.

When the data gap consisted of 3 points (hours) or less, linear interpolation was used to reconstruct the data. These small period data gaps constituted the majority of data gap instances.

Longer data gaps were extrapolated by applying a residual offset between an adjacent well timeseries which exhibited the largest correlation r^2_{xy} with the original timeseries. To examine correlation between the timeseries, ensemble averages of r^2_{xy} were computed based on data blocks in increments of 24 points (hours). If the total number of points in the timeseries is P, and N is the number of points in a block of data, then the number of ensemble averages is $M = (P/N - 1)$, and the corresponding correlations are given by:

$$\overline{r^2_{xy}} = \frac{1}{M} \sum_{i}^{M} r^2_{xy_i} \tag{1}$$

Figure 7 plots $\overline{r^2_{xy}}$ vs. data blocks of increasing size. It is not surprising that as the size of the data blocks increase, that the average correlation decreases between PBF-4 and PBF-5, however the lack of a decrease between the other two data sets is unexpected. The scale-free behavior of PBF-3 and PBF-4 to PBF-5 may indicate a short timescale decoupling between the upper layer (PBF-3) and the other, deeper zones of the Floridan aquifer

at this well site.

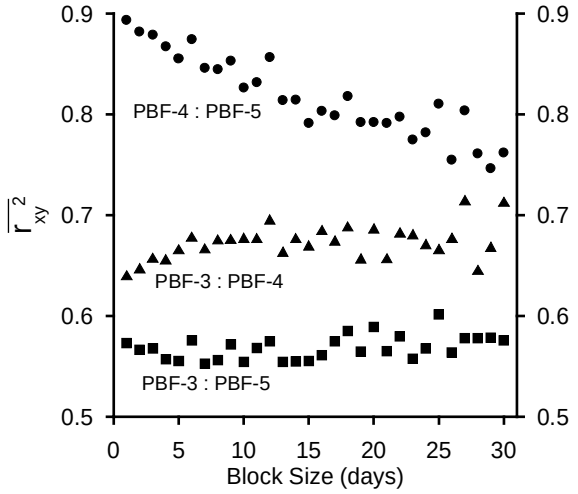

Figure 7: Averaged cross-correlation coefficients for data blocks of varying lengths.

The results shown in figure 7 were used as a decision tool in selection of which surrogate timeseries to use in the data extrapolation procedure. For example, in estimation of the PBF-5 data gaps, the data from PBF-4 was used as the correlated timeseries. Once the surrogate timeseries is identified, the offset value was constructed as follows:

1. Let i_- be the timeseries index of the start of the data gap.
2. Let i_+ be the timeseries index of the end of the data gap.
3. Compute an average offset for 50 points prior to the data gap: $\overline{\Omega_-} = \frac{1}{50} \sum_{i=i_-}^{i=i_-+50} (x_i - y_i)$
4. Compute an average offset for 50 points after the data gap: $\overline{\Omega_+} = \frac{1}{50} \sum_{i=i_+}^{i=i_++50} (x_i - y_i)$
5. Average the prior and post offsets for a single offset: $\overline{\Omega} = \left(\overline{\Omega_-} + \overline{\Omega_+}\right)/2$

Once the offset is computed, the extrapolated data $\hat{x_i}$ is estimated from the correlated data y_i:

$$\hat{x_i} = y_i + \overline{\Omega} \tag{2}$$

2.3 Coupled Response of Barometric Pressure, Aquifer Stage, and Ocean Stage

A short period plot of the barometric pressure, ocean water levels at Lake Worth Pier and aquifer stage from well PBF-5 are shown in figure 8. This data records the passage of hurricane Frances on September 5th, 2004. This graphic suggests a strong coupling between ocean water level changes and variation in aquifer well stage. Strong visualization of the inverse barometric effect on both the ocean [Apel, 1987] and well stages [Jacob, 1940] is also provided.

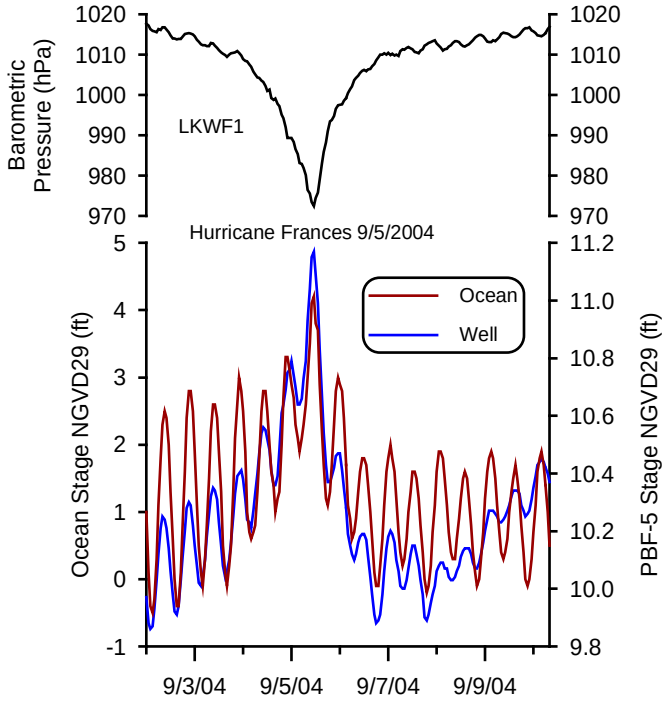

Figure 8: Snapshot of Lake Worth ocean tide and barometric pressure, well PBF-5 water level during the passage of hurricane Frances.

3 Aquifer Characterization from Tidal Forcing

There is a long history of recognition that geophysical forcings such as ocean tidal and atmospheric pressure couple into aquifer response. Over half a century ago, Ferris analyzed transmissivity of a semi-infinite, confined aquifer with a submerged suboutcropping driven by ocean tidal or other intersecting waterbody fluctuations with a diffusion formulation [Ferris, 1951]. A schematic depiction of the Ferris geometry is shown in figure 9.

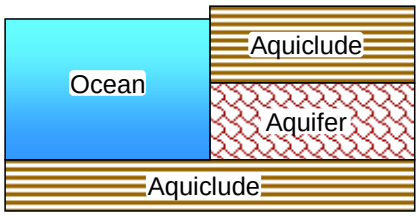

Figure 9: The work of Ferris assumed a confined aquifer with a submerged suboutcropping.

Two decades later, Van der Kamp considered the case where the confined aquifer extended beneath the tidal waterbody, and estimated specific storage and hydraulic conductivity based on the 'tidal efficiency' and time lags [Van der Kamp, 1972]. An illustration of the Van der Kamp geometry is shown in figure 10.

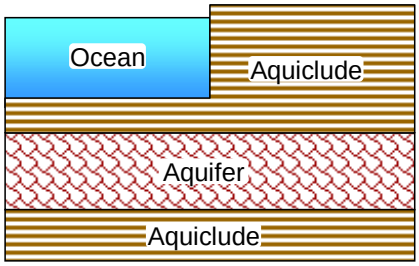

Figure 10: Van der Kamp assumed a confined aquifer extending underneath the ocean.

Application of modern digital signal processing and frequency domain analysis to characterization of aquifer well response was performed by Rojstaczer [Rojstaczer, 1988a]. Cross-spectral analysis of atmospheric pressure

to well stage, and earth tide to well stage transfer functions, as well as coherence to compute confidence intervals of barometric efficiency spectrums were introduced. A method for removing atmospheric loading effects by inversion of estimated frequency response functions of the atmospheric pressure into a timeseries, which is subtracted from the well timeseries was also demonstrated. Based on these methods, Rojstaczer estimated vertical pneumatic diffusivity of unsaturated zone, vertical hydraulic diffusivity of the saturated zone, and lateral permeability of the aquifer [Rojstaczer, 1988b].

Ritzi et. al. developed analytical transfer functions to model the combined earth tide and atmospheric forcing on well response. They demonstrate that the combined model improves the identification and precision of transmissivity parameter estimates in comparison to separate tide-well and atmospheric-well models. Based on composite transfer functions, they were able to provide an inverse modeling formulation for estimating transmissivity parameters [Ritzi, 1991].

A generalization of the Ferris and Van der Kamp models was proposed by Li and Jiao where the coastal aquifer may consist of leaky semiconfining layer separating an overlying unconfined aquifer from an underlying semiconfined aquifer [Li and Jiao, 2001]. This method estimates the hydraulic diffusivity, however, only analytical cases were considered. A pictorial representation of the Li & Jiao geometry is shown in figure 11.

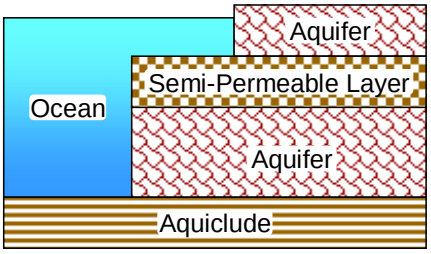

Figure 11: The work of Li & Jiao considered a generalized geometry with leakage between an unconfined surficial aquifer and a confined aquifer which suboutcrops to the ocean.

Recent work by Merritt has applied the methods of Van der Kamp, and Li & Jiao to characterization of Floridan aquifer properties along the southwest coast of Florida [Merritt, 2004]. We will follow the work of Merritt in the evaluation of coastal aquifer properties, however, estimates of the ocean tidal to well stage coupling coefficients will be computed directly from spectral amplitude components without resort to timeseries filtering or

regression analysis to estimate the spectral components. Transfer functions and coherence will be used to identify spectral modes which do not couple atmospheric forcings, without hand-fitting or application of analytically derived functions.

3.1 Diffusivity

3.1.1 Li & Jiao Diffusivity

Based on the generalization of [Li and Jiao, 2001], [Merritt, 2004] offers formula relating the transmissivity (T_W) and storage coefficient (S) of a tidally influenced aquifer at locations inland of the shoreline:

$$\frac{T_W}{S} = \frac{\pi p^2 x_o^2}{\tau \left[ln\left(\frac{r}{C_e}\right)\right]^2} = \frac{\pi q^2 x_o^2}{\tau(\Phi + \varphi)^2} \tag{3}$$

where p and q are aquifer vertical leakage parameters (if no vertical leakage $p = q = 1$, if leakage $p, q > 1$), x_o is distance from the shoreline to the aquifer well, τ the period of the tidal forcing component, r the ratio of aquifer well head to ocean tidal amplitudes, C_e an aquifer loading efficiency ($0 < C_e \leq 1$), Φ the phase-shift between the well stage and ocean tidal components, and φ a phase factor for leakage effects.

In this report, the amplitude ratio r is referred to as a coupling coefficient. These coupling coefficients will be computed from averaged power spectral densities in the frequency domain, with coherent power analysis used to identify frequencies which do not couple atmospheric forcing to the well response. The fact that signal power ratios determine r means that exact synchronization of the observations is not required. This is not the case for the phase-dependent formulation which includes the Φ term. To accurately determine Φ, exact synchronization and accuracy of the time measurements of the hydrological, meteorological and oceanographic data is required. While we do not have the luxury of synchronized data, examination of figure 8 suggests no discernible phase-lag (time-delay) between tidal and well response measurements on the scale of an hour.

3.1.2 Van der Kamp Diffusivity

Equation 3 reduces to the case considered by [Van der Kamp, 1972] when vertical leakage is zero and the aquifer extent under the sea is infinite ($p = q = 1, C_e = L_e/2, \varphi = 0$):

$$\frac{T_W}{S} = \frac{\pi x_o^2}{\tau \left[ln\left(\frac{2r}{L_e}\right)\right]^2} = \frac{\pi x_o^2}{\tau \Phi^2} \tag{4}$$

where L_e is the aquifer loading efficiency.

3.1.3 Ferris Diffusivity

In the case where the vertical leakage is zero, and the aquifer terminates as a suboutcropping at the sea interface ($p = q = 1, C_e = 1, \varphi = 0$)), equation 3 provides estimates consistent with [Ferris, 1951]:

$$\frac{T_W}{S} = \frac{\pi x_o^2}{\tau \left[ln\left(r\right)\right]^2} = \frac{\pi x_o^2}{\tau \Phi^2} \tag{5}$$

3.2 Specific Storage

Van der Kamp provides a relation between the specific storage S_s of an aquifer under the sea and the tidal efficiency T_e [Van der Kamp, 1969]:

$$S_s = \frac{\theta \ \beta \ \gamma_w}{1 - T_e} \tag{6}$$

where θ is the porosity of the aquifer, β compressibility of water, and γ_w the specific weight of water. The tidal efficiency satisfies $T_e + B_e = 1$ where B_e is the barometric efficiency of the aquifer. Thus, given estimates of the barometric efficiency, porosity, compressibility and specific weight, an estimate of specific storage is computable. If the vertical thickness of the aquifer Δz is known, then the storage coefficient S can be estimated:

$$S = \Delta z \cdot S_s \tag{7}$$

3.3 Barometric Efficiency

Barometric efficiency (B_e) quantifies coupling between changes in atmospheric pressure and aquifer piezometric heads. It characterizes aquifer confinement and elasticity, presence of borehole/skin effects, and pneumatic diffusivity in the unsaturated zone [Rasmussen, 1997]. B_e is therefore a prominent parameter in estimates of transmissivity, storage and other aquifer properties.

Clark's method has been shown to provide an unbiased and consistent estimate of barometric efficiency [Davis, 1993]. Clark's method assumes that

an incremental change in aquifer head is attributed to an incremental change in atmospheric pressure.

Atmospheric pressure variations exhibit well defined diurnal and semi-diurnal frequencies, as well as shorter timescale variations from atmospheric dynamics. These timescales are typically much smaller than those of aquifer head variations from recharge or leakage. For example, in figure 6 the short timescale variations are clearly of a much higher frequency than the long term aquifer stage changes. Subsequently, assumption of coherence between changes in atmospheric pressure and aquifer head at short timescales is usually reasonable. Figure 12 plots the barometric efficiencies for the 4 wells computed with Clark's method.

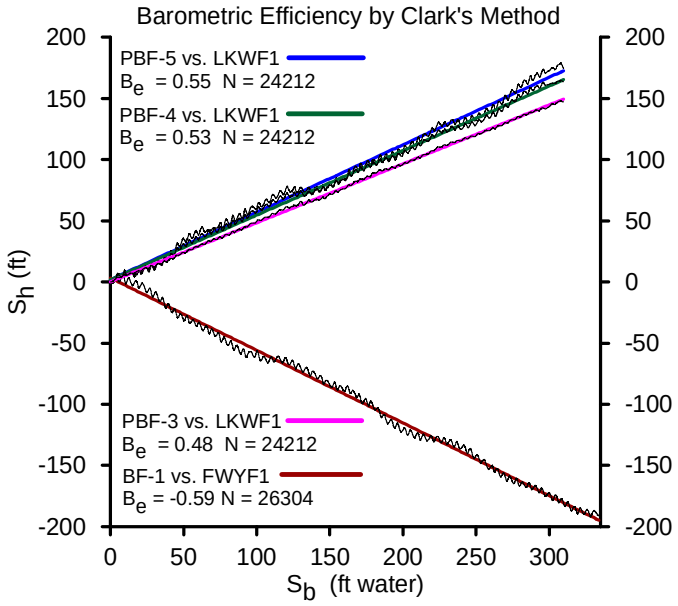

Figure 12: Clark's linear regression of well stage change vs. barometric pressure change estimates of aquifer barometric efficiencies.

While the PBF wells produce consistent estimates with values from 48% to 55%, BF-1 does not maintain the inverse barometric pressure to aquifer stage relationship assumed by the method. This indicates that either the data records are not properly synchronized, or that some other forcing mechanism is driving the aquifer stage variations. Further, from observation of the strong couplings observed between the tidal and well stages in figure

8, one would expect loading efficiencies greater than 50%. For example, a rough estimate of B_e can be manually computed from an 'eyeball' estimate of well stage change in response to a 30 hPa change in barometric pressure (1005 - 975 hPa) both before, and after hurricane Frances from figure 8. This produces estimates of $B_e = 0.68$ (before) and $B_e = 0.78$ (after).

The discrepancies noted above indicate that we should estimate barometric efficiency over timescales where ocean tidal forcing is not observed. To that end, an estimate of the barometric efficiency over a timescale of 4 days with a long period increase in barometric pressure can be computed from the ratio of slopes of least-squares regression fits to the well stages and barometric pressure. The corresponding plots are shown in figures 13 - 16. Results of the Clark method and the least squares (LS) are presented in table 2.

Well	Clark B_e	LS B_e
PBF-3	0.48	0.71
PBF-4	0.53	0.72
PBF-5	0.55	0.67
BF-1	-0.59	0.59

Table 2: Estimates of barometric efficiency from least squares (LS) fits of well stage and barometric pressure variations over a 4-day period.

The PBF wells are found to have $B_e \approx 0.7$. This result is consistent with the estimate obtained from the hurricane Frances event, and indicate that tidal forcings in these coastal wells is strong enough to invalidate the application of Clark's method for estimates of B_e when based on hourly data.

An examination of spectral analysis which isolates tidal forcing from the barometric variations applied to estimation of B_e is discussed in section 4.5.

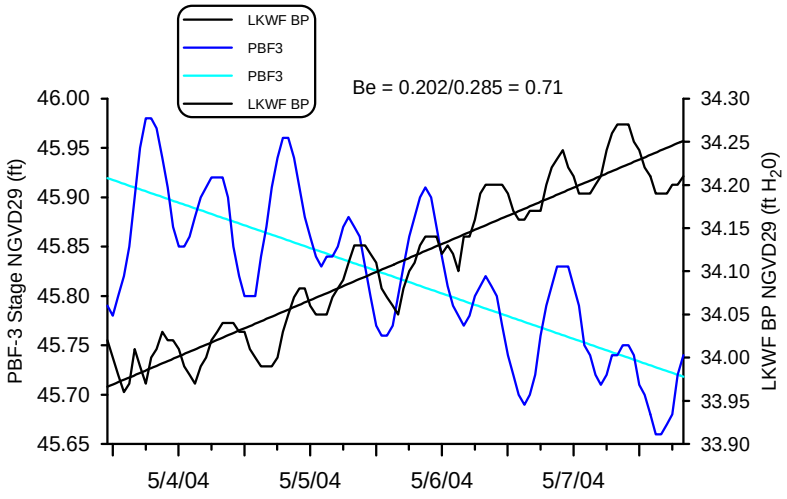

Figure 13: Timeseries of PBF-3 well stage and Lake Worth barometric pressure used to estimate barometric efficiency.

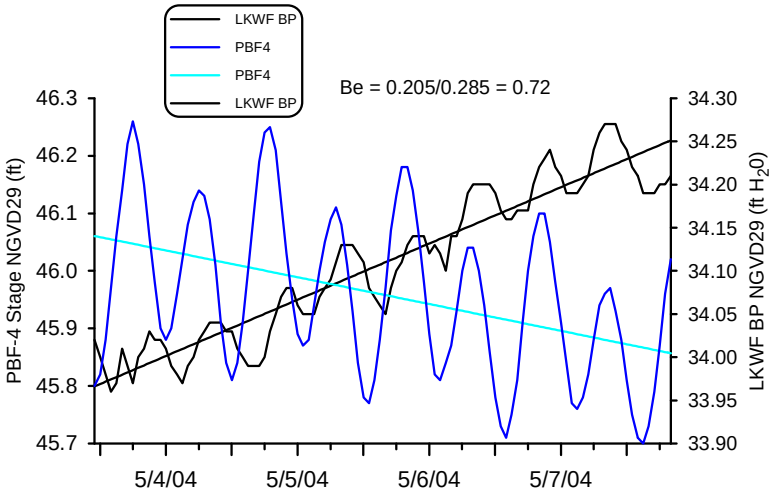

Figure 14: Timeseries of PBF-4 well stage and Lake Worth barometric pressure used to estimate barometric efficiency.

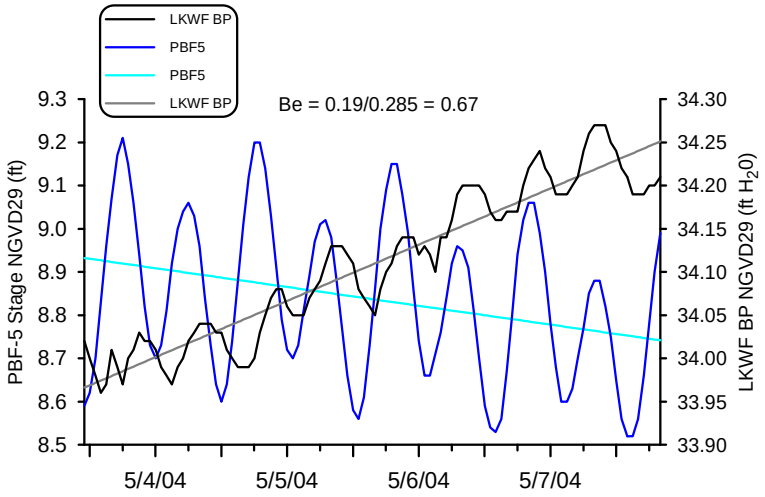

Figure 15: Timeseries of PBF-5 well stage and Lake Worth barometric pressure used to estimate barometric efficiency.

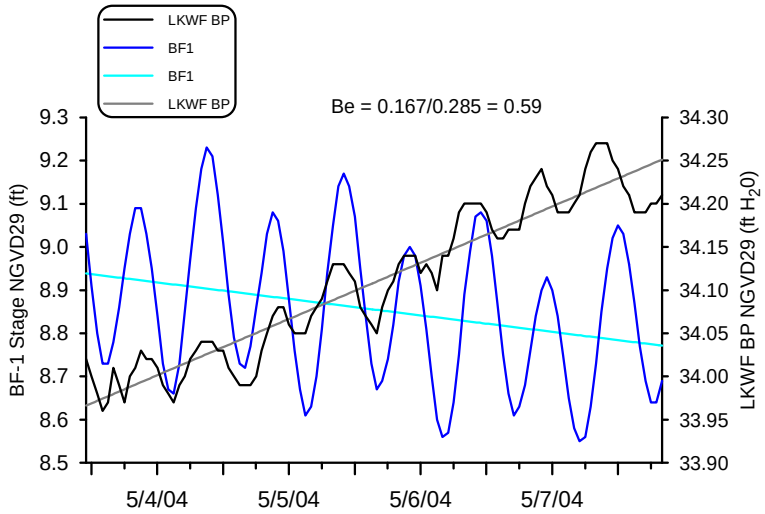

Figure 16: Timeseries of BF-1 well stage and Lake Worth barometric pressure used to estimate barometric efficiency.

4 Spectral Analysis

In this and the following section, we examine spectral density functions computed from the atmospheric pressure, ocean water level, and aquifer well stages in order to determine coupling between these variables. The goal is to identify power amplitude ratios (coupling coefficients) between the ocean and aquifer stages for use in equations 3, 4 and 5 to estimate aquifer flow properties. Isolation of ocean-to-aquifer coupling will depend upon identification of frequencies which do not couple barometric forcings.

The discussions are based on the one-sided spectral density functions denoted $G_{\mathrm{xy}}(f)$, where x and y denote two observable timeseries. Functional notation of dependence on the frequency parameter f will be suppressed in the remaining sections.

We employ standard frequency analysis processing with suppression of spectral sidelobe leakage between ensemble averages by application of a Hanning window to each processed data block. Overlapped processing is applied to compensate spectral amplitude variance introduced by the window. For a review of spectral density functions and their estimation procedures, the reader may consult [Bendat, 1986].

4.1 Spectral Resolution and Uncertainty

Here we establish some basic properties of the spectral analysis frequency and amplitude resolution. The frequency resolution Δf defines how closely two distinct frequency components can be resolved, and is defined by: $\Delta f = 1/(N\Delta t)$ where Δt is the sampling interval and N the number of points in a block of data. Usually, Δt is fixed based on the Nyquist frequency, hardware limitations, or data availability. Therefore, for maximal spectral resolution the number of points in a block of data should be as large as possible. However, if all of the data are analyzed in a single block ($N = P$), the amplitude accuracy is poor. To reduce the amplitude error, the data are subdivided into M ensembles, which are averaged to increase the amplitude accuracy. Thus there is a trade off between spectral resolution and amplitude accuracy.

In the current analysis, when no ensemble averaging is used ($N = P, M = 0$), the spectral resolution is: Δf_P=1.1473E-8 Hz (9.9124E-4 cycle/day). With a data overlap of $v \in [0, 1]$, the number of ensemble averages is $M = P/(N \cdot v) - 1$. Therefore, if the P data points are processed with a 50% overlap resulting in $M = 10$ ensemble averages, the resolution is: Δf_M=6.3131E-8 Hz (5.4544E-3 cycle/day). Thus, with ensemble averaging

the frequency resolution is decreased by a factor of 6.

Considering the dominant tidal frequency modes listed in table 3, the minimum frequency separation between modes is Δf_{min}=5.207500E-8 Hz. Since this minimum frequency separation is smaller than Δf_M, at least two modes will lose spectral distinction when ensemble averaging is used. However, when spectral averaging is not used, the resolution bandwidth is sufficient to resolve all tidal modes.

Mode	Frequency (Hz) x10^{-5}	Frequency (cycle/day)	Period (hr)
Q_1	1.033847	0.893244	26.868357
$\mathbf{O_1}$	1.075852	0.929536	25.819341
M_1	1.118572	0.966446	24.833249
$\mathbf{K_1}$	1.160576	1.002738	23.934469
$2N_2$	2.152419	1.859969	12.905375
μ_2	2.158041	1.864547	12.871758
$\mathbf{N_2}$	2.194424	1.895982	12.658348
$\mathbf{M_2}$	2.236428	1.932274	12.420602
L_2	2.278432	1.968565	12.191620
$\mathbf{S_2}$	2.314815	2.000000	12.000000
K_2	2.321153	2.005476	11.967235

Table 3: Ocean tidal spectral components. The five major modes (in bold) account for 95% of the tidal energy.

Of course, the loss in spectral resolution from ensemble averaging is offset by a gain in power amplitude resolution. Spectral amplitude estimates are usually considered to contain two sources of error: a bias error ϵ_B, and a random error ϵ_R. The bias error is primarily dependent on the resolution bandwidth: $\epsilon_B \approx \Delta f^2$. In the present case Δf is small enough such that ϵ_B can be safely ignored.

The normalized random error for autospectral estimates (G_{xx}) is given by:

$$\epsilon_R = \frac{1}{\sqrt{M}} \tag{8}$$

and for cross spectral estimates (G_{xy}) by:

$$\epsilon_R = \frac{1}{|\gamma_{\mathrm{xy}}|\sqrt{M}} \tag{9}$$

where γ_{xy} is the spectral coherence (to be defined in section 5.1). For the present analysis with $M = 10$, the error in autospectral amplitude estimates will be reduced by a factor of 3 compared to the spectrums without ensemble averaging. It is also clear that cross-spectral amplitudes require high coherence ($\gamma \rightarrow 1$) to take full advantage of the decrease in random amplitude errors from averaging.

4.2 Autospectral Density

The power autospectral density (PSD) of the Lake Worth Pier ocean water level data of figure 3 is shown in figure 17. Units are decibels referenced to feet (NGVD29) squared per Hertz, (dB\\ ft^2/Hz), which express a logarithmic ratio of signal power on a normalized frequency basis. The background (red) data is the non-ensemble averaged PSD estimate, while the foreground trace (blue) is the overlapped, ensemble averaged estimate. The differences in frequency and amplitude resolutions between the two are as expected. The non-averaged PSD (red) spectrum clearly resolves many of the tidal modes (Q_1, O_1, M_1, K_1, $2N_2$, N_2, M_2, L_2, K_2), though the amplitude variance is evident in the noise floor. The averaged PSD estimates (blue) clearly show smaller amplitude noise variance, and the inability to separately resolve mode $2N_2$ from μ_2; as well as S_2 from K_2. The averaged estimates display impressive signal-to-noise (SNR) ratios in excess of 20 dB for modes O_1, K_1, N_2, M_2.

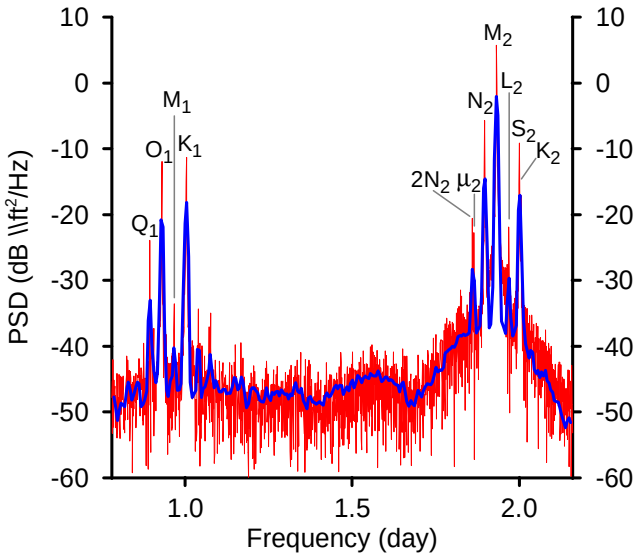

Figure 17: Autospectral power density of Lake Worth ocean water stage.

Figure 18 plots PSD of the Lake Worth Pier barometric pressure data. To maintain consistent basis with the ocean and aquifer well stages, the pressure data was converted to feet of water (NGVD29). Again, the background trace (red) is the non-averaged PSD with maximal spectral resolution and the foreground plot (blue) the ensemble averaged estimate. The dominant features are the diurnal and semi-diurnal modes labeled S_1 and S_2. The S_1 mode is not a tidal frequency, though it is very close in frequency to K_1, while S_2 has exactly the same frequency as the S_2 tidal component. A small contribution of atmospheric tide at M_2 is also observed [Chapman, 1970].

As suggested earlier, the atmospheric pressure forcing couples to both the ocean and aquifer responses. In the pursuit to identify ocean - aquifer forcings without atmospheric influence, this spectrum provides the initial indication that frequencies S_1, S_2 and M_2 are to be avoided.

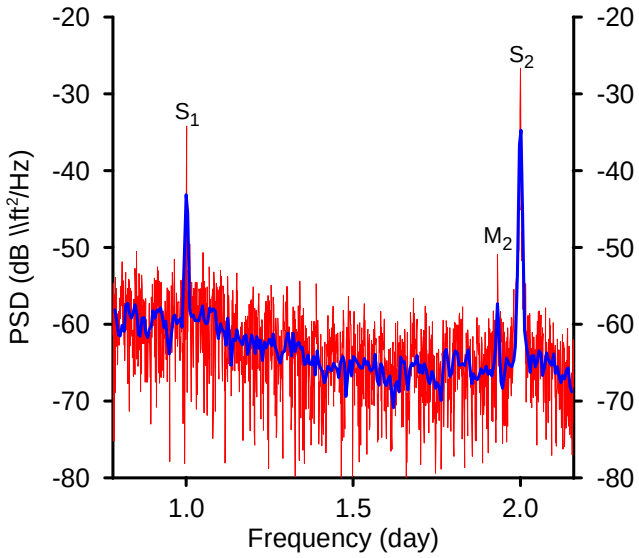

Figure 18: Autospectral power density of Lake Worth barometric pressure.

The PSD of Floridan Aquifer well PBF-5 is plotted in figure 19. There is remarkable similarity to the PSD of Lake Worth Pier ocean stage in figure 17, notably, all of the tidal modes identified in the ocean spectrum are observable in the well data if no ensemble averages are performed. However, with reduced error in spectral amplitudes from averaging, tidal modes M_1 and L_2 have little or no signal-to-noise ratio. Nonetheless, the large signal-to-noise ratios of the other tidal modes clearly indicate strong coupling between the ocean tides and/or atmospheric forcing, and the well response.

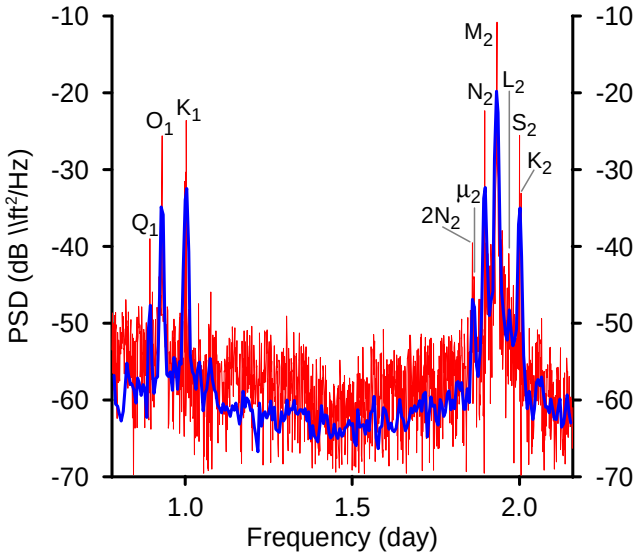

Figure 19: Autospectral power density of well PBF-5 water stage.

4.3 Spectral Amplitudes

The following tables publish power spectral amplitudes obtained from ensemble averaged PSD estimates at the five primary tidal modes for the ocean and aquifer well stages. Table 4 list amplitudes of the Lake Worth Pier ocean water level, corresponding to data of figure 17.

Mode	G_{xx} (dB)	G_{xx} (ft)
O_1	-20.81	0.09100
K_1	-18.15	0.12374
N_2	-14.61	0.18599
M_2	- 2.05	0.78977
S_2	-17.10	0.13964

Table 4: Ocean tidal spectral amplitudes.

Amplitudes of the upper Floridan Aquifer well PBF-3 stage response at the five primary tidal modes are listed in table 5.

Mode	G_{xx} (dB)	G_{xx} (ft)
O_1	-39.37	0.010752
K_1	-37.45	0.013412
N_2	-42.15	0.007807
M_2	-29.82	0.032285
S_2	-41.84	0.008091

Table 5: PBF-3 spectral amplitudes.

Amplitudes of the middle Floridan Aquifer well PBF-4 stage are listed in table 6.

Mode	G_{xx} (dB)	G_{xx} (ft)
O_1	-36.36	0.015205
K_1	-34.07	0.019792
N_2	-34.86	0.018072
M_2	-22.24	0.077268
S_2	-38.63	0.011708

Table 6: PBF-4 spectral amplitudes.

Lower Floridan Aquifer well (PBF-5) amplitudes are presented in table 7. These levels are taken from the data plotted in 19.

Mode	G_{xx} (dB)	G_{xx} (ft)
O_1	-34.86	0.018072
K_1	-32.44	0.023878
N_2	-32.34	0.024155
M_2	-19.82	0.102094
S_2	-35.02	0.017742

Table 7: PBF-5 spectral amplitudes.

Amplitudes of the lower Floridan Aquifer well BF-1 stage are listed in table 8.

Mode	G_{xx} (dB)	G_{xx} (ft)
O_1	-35.04	0.017701
K_1	-31.70	0.026002
N_2	-32.51	0.023686
M_2	-19.81	0.102212
S_2	-36.35	0.015223

Table 8: BF-1 spectral amplitudes.

4.4 Cross Spectral Phase

Examination of the hydrological analytical models expressed in section 3.1 reveal two independent formulations for estimation of diffusivity. The first is based on amplitude coupling coefficients (r), the second on relative phase (Φ) between the tidal forcing and well response (equation 4).

The phase can be extracted directly from the cross-spectral density G_{TW} between the tidal forcing and the well response. (Refer to equation 12 for definition of cross-spectral density.) G_{TW} is composed of a real valued coincident (co-spectrum) and imaginary quadrature (quad-spectrum): $G_{\mathrm{TW}} = C_{\mathrm{TW}} + \mathrm{j}Q_{\mathrm{TW}}$, the spectral phase function is given by [Bendat, 1986]:

$$\Phi = \tan^{-1}\left(\frac{Q_{\mathrm{TW}}}{C_{\mathrm{TW}}}\right) \tag{10}$$

Figure 20 plots the phase for the ocean tidal to PBF wells at the diurnal frequency mode O_1. The thick black line is the autopsectral density of PBF-5, which is included for reference. One can see that 'within' the frequencies contributing power to mode O_1, the phase values are relatively uniform.

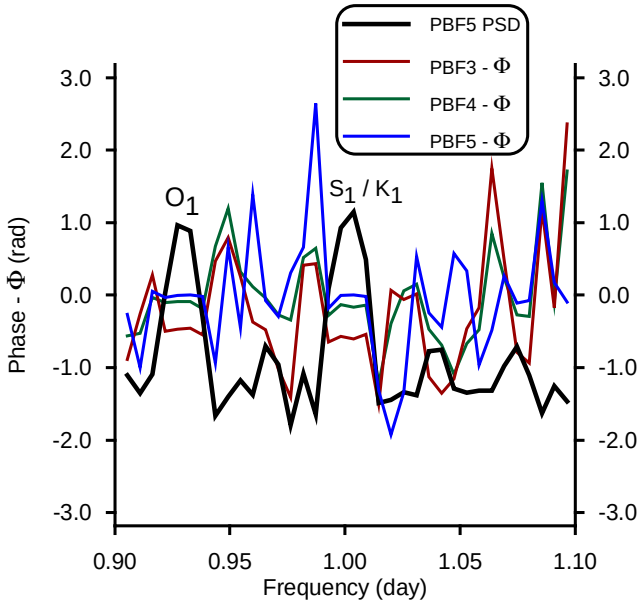

Figure 20: Cross-spectral phase of LKWF tide to PBF well water stage at diurnal modes.

At the semi-diurnal modes N_2 and M_2, the spectral phase results are plotted with the reference autopsectral density of PBF-5 in figure 21.

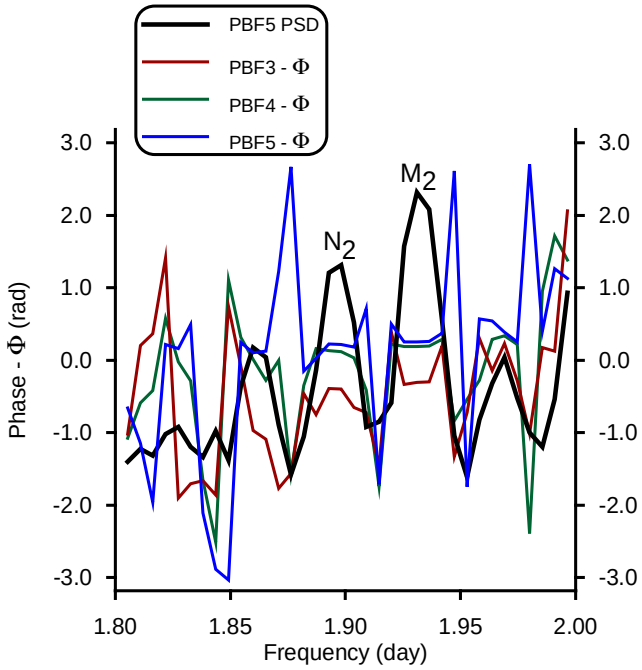

Figure 21: Cross-spectral phase of LKWF tide to PBF well water stage at semi-diurnal modes.

As is the case with the O_1 mode, the phase-lags of the N_2 and M_2 modes are relatively uniform in value within the power frequencies of the respective modes. Tabulated values for the phase components at the PBF-3, 4, 5 wells are shown in table 9.

Mode	PBF-3	PBF-4	PBF-5
O_1	-0.4664	-0.0916	-0.0045
N_2	-0.3967	0.1124	0.2144
M_2	-0.3083	0.1883	0.2483

Table 9: Spectral Phase Values (radians).

4.5 Barometric Efficiency by Spectral Method

Having established that estimates of B_e via Clark's method in tidally forced wells are questionable (section 3.3), a natural question is: can B_e be estimated from spectral amplitudes which do not couple tidally forced frequencies?

As we have seen from table 3 and figure 18, the diurnal barometric pressure mode S_1 is the only atmospheric pressure component which does not alias an ocean tidal mode. Therefore, if the S_1 spectral amplitudes of barometric pressure and well stage variance can be estimated, their ratio should give an estimate of B_e which has no ocean tidal influence.

To decide whether or not this is possible with the current data set, we first examine averaged power spectral densities of PBF well stages and Lake Worth barometric pressure in figure 22.

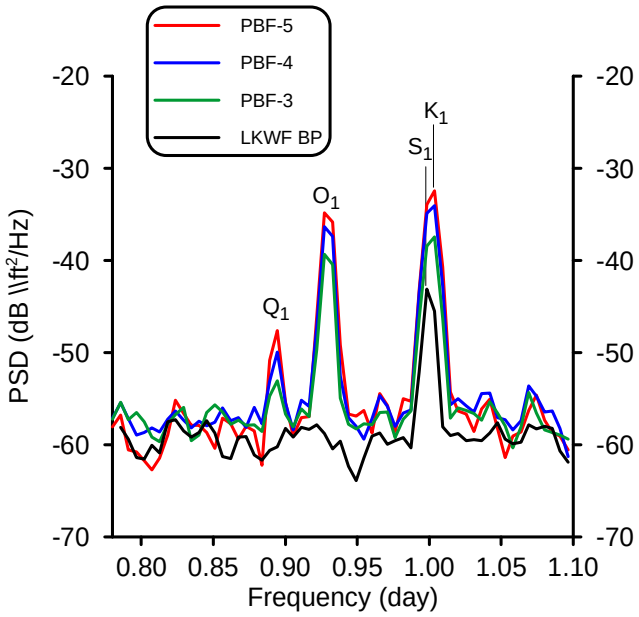

Figure 22: Averaged power spectral densities of PBF well stage and Lake Worth barometric pressure.

It is clear from figure 22 that the S_1 is not distinctly resolved from the K_1 tidal mode, therefore, we have insufficient spectral resolution to attempt estimation of B_e.

To examine maximal spectral resolution, we employ a single FFT spec-

trum, and zoom in on the frequency band of interest, as shown in figure 23. Here we see that there is sufficient spectral resolution to isolate the S_1 barometric pressure variation from the ocean tidal components. However, it is also clear that estimates of B_e will result in barometric efficiencies greater than 1, as all of the well stage variances are greater than the barometric pressure variance at S_1. This suggests either an amplification of well response from the barometric forcing at a frequency of S_1, or, that assumption of linear independence between the barometric pressure and well response is not satisfied. As will be seen in section 5.4, the latter condition appears to apply. Therefore, we must conclude that for this data set with coastal wells strongly influenced by ocean tidal forcings, spectral methods are not suitable for estimation of B_e directly from barometric pressure forcing.

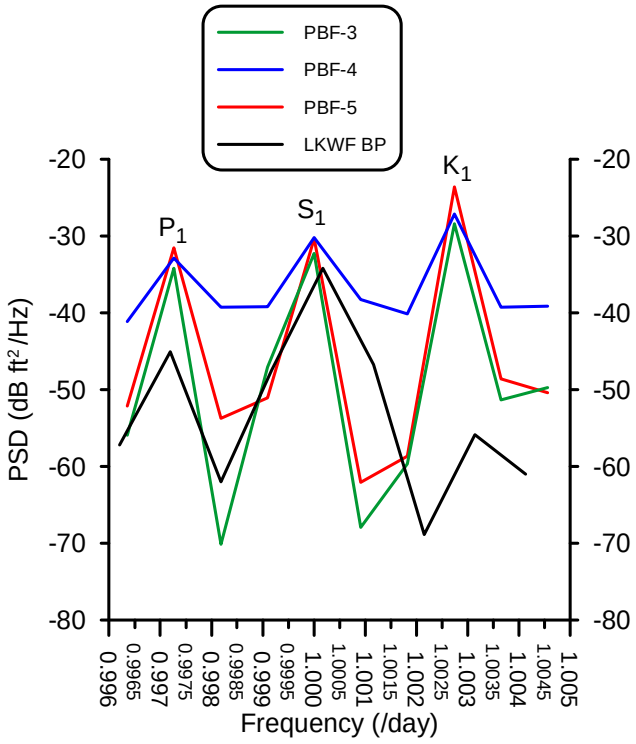

Figure 23: Single FFT power spectral densities of PBF well stage and Lake Worth barometric pressure.

5 Linear System Frequency Response Functions

In this section we apply linear systems theory in the frequency domain to estimate transfer functions and coherence between atmospheric/tidal forcing, and aquifer well response.

Inherent in a linear system transformation is the impulse response function $h(t)$ that convolves an input $\mathrm{x}(t)$ to an output: $\mathrm{y}(t) = h(t) \star \mathrm{x}(t)$, where the usual superposition and homogeneity properties are assumed. Superposition simply implies $h(x + y) = h(x) + h(y)$, while homogeneity ensures $h(\alpha x) = \alpha h(x)$. Additionally, shift-invariance is assumed to ensure uniqueness of the impulse response. Transformation to the frequency domain replaces convolution with multiplication: $G_{\mathrm{y}} = H_{\mathrm{xy}} \cdot G_{\mathrm{x}}$. The frequency response is the system transfer function, usually represented as:

$$H_{\mathrm{xy}} = \frac{G_{\mathrm{y}}}{G_{\mathrm{x}}} \tag{11}$$

which is related to the cross-spectral density G_{xy} between x and y:

$$H_{\mathrm{xy}} = \frac{G_{\mathrm{y}}}{G_{\mathrm{x}}} \cdot \frac{G_{\mathrm{x}}^*}{G_{\mathrm{x}}^*} = \frac{G_{\mathrm{xy}}}{G_{\mathrm{xx}}} \tag{12}$$

where * denotes complex conjugation.

5.1 Coherence

Considering a SISO linear system described above, the coherence function between the input and output is defined as:

$$\gamma_{\mathrm{xy}}^2 = \frac{|G_{\mathrm{xy}}|^2}{G_{\mathrm{xx}} G_{\mathrm{yy}}} \tag{13}$$

Coherence satisfies $0 \leq \gamma_{\mathrm{xy}}^2 \leq 1$, and in the ideal case of a noiseless, constant parameter SISO linear system, $\gamma_{\mathrm{xy}}^2 = 1$. In the event that the input/output are completely unrelated $\gamma_{\mathrm{xy}}^2 = 0$. For values of γ_{xy}^2 between zero and one, three possibilities exist:

1. Noise is being introduced to the measurements.
2. The system is not linear.
3. Output $\mathrm{y}(t)$ results from input $\mathrm{x}(t)$ as well as other inputs.

If the system is linear, γ_{xy}^2 represents the fractional portion of the output power that is contributed by the input at each frequency. This property

has potential to serve as a powerful diagnostic in the identification of signal propagation through a linear system.

5.2 SISO Ocean to Aquifer Coherence

Returning to the coupled system depiction shown in figure 1, a simplistic linear system to investigate the ocean-aquifer coupling would be to assign ocean stage (T) to the input, and well stage (W) to the output, as depicted in figure 24.

Figure 24: A single-input single-output (SISO) linear system.

Coherence of this system with ocean tidal stage at Lake Worth Pier (T) and aquifer well stage PBF-5 (W), is plotted in figure 25. Significant power coupling is seen at many of the tidal modes, indicating that coupling coefficient estimation at these frequencies would have small amplitude errors, and that the ocean tidal forcing dominates the well response at these modes. However, the simple model has not accounted for common-mode coupling of the barometric pressure, therefore it is not clear which of these modes can best isolate the ocean-aquifer coupling. This question will be addressed in the following sections. Numeric values of SISO coherence for selected tidal modes are shown in table 10.

Mode	PBF-3	PBF-4	PBF-5	BF-1
O_1	0.9880	0.9896	0.9895	0.9944
K_1	0.7438	0.7394	0.8743	0.6529
N_2	0.9578	0.9867	0.9899	0.9956
M_2	0.9853	0.9988	0.9969	0.9995
S_2	0.8586	0.9352	0.9696	0.9749

Table 10: Lake Worth ocean to PBF well SISO coherence.

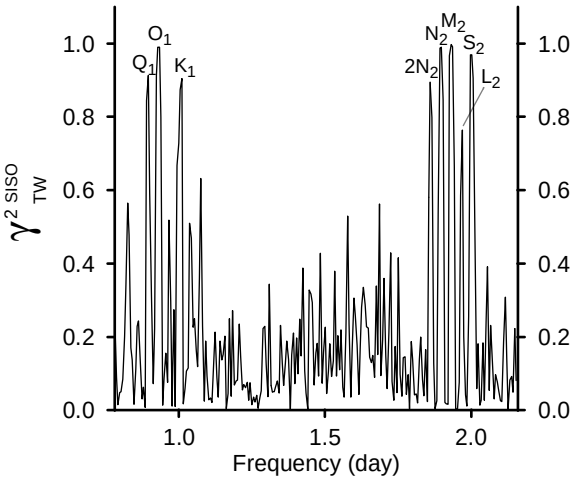

Figure 25: Coherence between Lake Worth ocean water stage and well PBF-5 water stage for a SISO model.

5.3 SIDO Ocean to Aquifer Coherence

The SISO model for the ocean-aquifer interaction encapsulates all signal energy into a single transfer function. This prevents isolation of barometric pressure effects from the ocean-aquifer coupling. One model which accounts for dual forcing of atmospheric pressure onto ocean and aquifer response is a single-input dual-output (SIDO) system with atmospheric pressure input (A), ocean tidal (T) and well outputs (W). Such a system is depicted in figure 26.

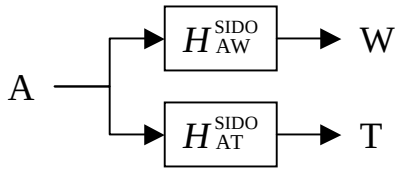

Figure 26: A single-input dual-output (SIDO) linear system.

Identification of common-mode forcing from the input A to the outputs W and T can be assessed by computation of coherence between the two outputs:

$$\gamma^2{}^{\text{SIDO}}_{\text{WT}} = \frac{|G_{\text{WT}}|^2}{G_{\text{WW}} G_{\text{TT}}} = \gamma^2{}^{\text{SIDO}}_{\text{AW}} \gamma^2{}^{\text{SIDO}}_{\text{AT}} \tag{14}$$

A high value of $\gamma^2{}^{\text{SIDO}}_{\text{WT}}$ indicates that W and T can be attributed to a common source A, and that noise is small compared to the signals. Figure 27 plots $\gamma^2{}^{\text{SIDO}}_{\text{WT}}$ and the two constituent coherences $\gamma^2{}^{\text{SIDO}}_{\text{AW}}$ and $\gamma^2{}^{\text{SIDO}}_{\text{AT}}$ where A and T represent the barometric pressure and ocean stage at Lake Worth Pier, W the well response at PBF-5. Two significant modes, M_2 and S_2 are identified as having a common atmospheric forcing, and should not be included in quantification of coupling coefficients which isolate the ocean-aquifer forcing. The presence of the M_2 mode is consistent with it's appearance in the PSD of Lake Worth Pier atmospheric pressure (figure 18), though there is not a clear physical mechanism by which this mode should couple into the barometric pressure measurements. Speculation for M_2 coupling could include earth-tide forcing of the pressure transducer, or a common-mode electronic coupling between the tide and barometric pressure recorders.

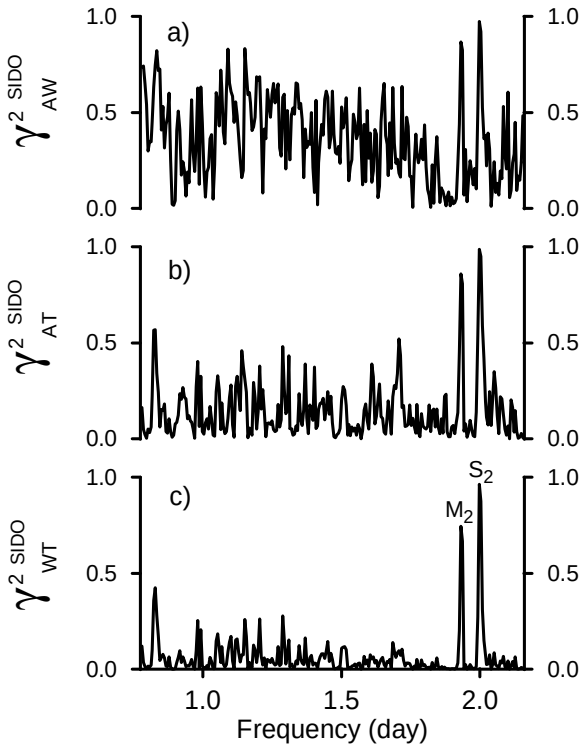

Figure 27: Coherence spectrums from the linear system of figure 26: a) $\gamma^2{}_{\mathrm{AW}}^{\mathrm{SIDO}}$ b) $\gamma^2{}_{\mathrm{AT}}^{\mathrm{SIDO}}$ c) $\gamma^2{}_{\mathrm{WT}}^{\mathrm{SIDO}}$.

5.4 Coupled DISO Ocean to Aquifer Transfer Function

A more complete model to represent the coupled forcings depicted in figure 1 is shown in figure 28. This model allows isolation of atmospheric pressure-aquifer forcing from the ocean-aquifer forcing with the two transfer functions $H_{\mathrm{AW}}^{\mathrm{DISO}}$ and $H_{\mathrm{TW}}^{\mathrm{DISO}}$.

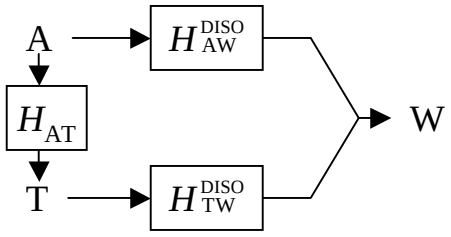

Figure 28: A coupled dual-input single-output (DISO) linear system.

The transfer functions can be computed from the auto and cross-spectral densities as follows:

$$H_{\mathrm{AW}}^{\mathrm{DISO}} = \frac{G_{\mathrm{AW}}\left[1 - \frac{G_{\mathrm{AT}}G_{\mathrm{TW}}}{G_{\mathrm{TT}}G_{\mathrm{AW}}}\right]}{G_{\mathrm{AA}}\left(1 - \gamma_{\mathrm{AT}}^2\right)} \tag{15}$$

$$H_{\mathrm{TW}}^{\mathrm{DISO}} = \frac{G_{\mathrm{TW}}\left[1 - \frac{G_{\mathrm{TA}}G_{\mathrm{AW}}}{G_{\mathrm{AA}}G_{\mathrm{TW}}}\right]}{G_{\mathrm{TT}}\left(1 - \gamma_{\mathrm{AT}}^2\right)} \tag{16}$$

$H_{\mathrm{TW}}^{\mathrm{DISO}}$ isolates ocean-aquifer response from direct atmospheric forcing of the aquifer. To examine this separation we may consider the effects of the simple SISO system of figure 24 in relation to that of the decoupled system of figure 28, by comparing the output spectrum G_W from each system. G_W can be computed from equation 11 with each of the system functions:

$$G_{\mathrm{W}}^{\mathrm{SISO}} = H_{\mathrm{TW}}^{\mathrm{SISO}} G_{\mathrm{T}} \tag{17}$$

$$G_{\mathrm{W}}^{\mathrm{DISO}} = H_{\mathrm{TW}}^{\mathrm{DISO}} G_{\mathrm{T}} \tag{18}$$

To compare outputs of equations 17 and 18, the difference spectrum of these two equations is plotted in figure 29. This figure quantifies the difference in contribution of the atmospheric pressure forcing on the well stages between the SISO and DISO system models. Two modes are identified

where the deviation is significant: S_1 and S_2, with a smaller deviation at M_2. This indicates that within linear system assumptions, atmospheric forcing of these three modes couples into the aquifer well response.

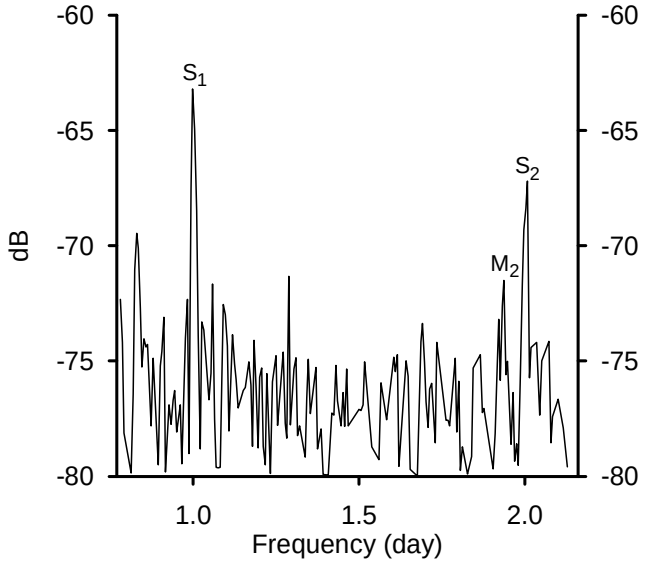

Figure 29: Power spectrum difference of well stage output, $G_{\mathrm{W}}^{\mathrm{SISO}}$ - $G_{\mathrm{W}}^{\mathrm{DISO}}$, quantifying atmospheric pressure forcing difference between $H_{\mathrm{TW}}^{\mathrm{SISO}}$ and $H_{\mathrm{TW}}^{\mathrm{DISO}}$.

5.5 Ocean-Aquifer Coupling Spectral Modes

Having explored the spectral response of aquifer well stage in relation to ocean tidal and atmospheric pressure modes, the following conclusions are made:

1. When ensemble averaged PSD estimates are computed, there is insufficient spectral resolution to isolate tidal mode $2N_2$ from μ_2, and atmospheric mode S_1 from tidal mode K_1. Additionally, the exact coincidence of barometric component S_2 with tidal component K_2 prevents separation of the source energy.
2. Coherence and transfer function analysis of SISO, SIDO and DISO models indicate that barometric modes S_1 and S_2, as well as tidal

mode M_2 couple energy from the atmospheric pressure forcing into the aquifer well response.

These results indicate that only two of the candidate tidal modes should be used to estimate ocean-aquifer coupling coefficients: O_1 and N_2. However, recognition of signal power ratios of the M_2 component are such that one might consider this mode as valid, assuming linearity applies. For example, the Lake Worth Pier tidal M_2 component has a SNR in excess of 30 dB, while the PBF-5 well M_2 SNR exceeds 25 dB. However, the barometric pressure SNR is approximately 6 dB. Considering these power ratios in linear terms, the values would be respectively: 1000, 316, and 4. Thus there are roughly two and three orders of magnitude greater signal power in the tidal and well data compared to the barometric pressure. In the absence of nonlinear coupling, such power ratios indicate that the atmospheric coupling of the M_2 can be safely ignored.

Based on these conclusions, table 11 summarizes the status of each of the tidal modes as suitable for isolation of ocean-aquifer coupling from the atmospheric forcing, while providing high signal-to-noise ratios and frequency resolution.

Mode	Limitation	Usable
Q_1	SNR	No
O_1		Yes
K_1	spectral resolution	No
M_1	SNR	No
$2N_2$	spectral resolution	No
μ_2	spectral resolution	No
N_2		Yes
L_2	SNR	No
M_2	Atmospheric coupling	Yes
S_2	Atmospheric coupling	No
K_2	spectral resolution	No

Table 11: Status of tidal modes for use in isolation of ocean-aquifer coupling.

6 Aquifer Property Estimation

This section applies results of the spectral data analysis (section 4) to estimate the aquifer transport based on the three analytical hydrological models described in section 3.

6.1 Coupling Coefficients

The ocean-aquifer coupling coefficients quantify the power ratio of discrete spectral components between the ocean tidal forcing and well stage response. The coefficients therefore represent the factor r in equations 3, 4 and 5.

Table 12 presents values of r for each of the four aquifer wells, at each of the five primary tidal spectral frequencies. The values are simply obtained from ratios of the spectral amplitudes presented in tables 4 - 8. For example, the O_1 value of r with respect to well PBF-3 is computed by dividing the Lake Worth Pier O_1 Tidal component of table 4 by the PBF-3 O_1 spectral amplitude from table 5: $r = 0.010752/0.09100 = 0.118$.

Mode	PBF-3	PBF-4	PBF-5	BF-1
O_1	0.118	0.167	0.198	0.194
K_1	0.108	0.160	0.193	0.210
N_2	0.042	0.097	0.130	0.127
M_2	0.041	0.098	0.129	0.129
S_2	0.058	0.084	0.127	0.109

Table 12: Ocean tidal - well coupling coefficients (r).

6.2 Time Lags

The phase values of section 4.4 provide values of Φ for equations 3, 4 and 5. These values can also be used to estimate the time-lag between the ocean tidal forcing and the aquifer well response. It is assumed that the phase-shift is linearly proportional to time-lag (τ) at each frequency: $\Phi = 2\pi f\tau = \omega\tau$, allowing evaluation of τ given Φ and frequency. Table 13 lists the computed time-lags at the major tidal modes.

Most of the values are negative, which is as expected, the tidal data 'leads' the well response (recall that the cross-spectrums were computed between the tidal input and well output: G_{TW}). It is interesting to note that these time-lags are generally less than 1 hour. This is consistent with

Mode	PBF-3	PBF-4	PBF-5
O_1	-1.99	-0.39	-0.02
K_1	-2.38	-0.66	-0.30
N_2	-0.80	0.23	0.43
M_2	-0.61	0.37	0.49

Table 13: Ocean tidal - well time-lags (τ) in hours.

examination of the ocean tidal and aquifer well timeseries which show less than one hour difference between the forcing and response (i.e. figure 8). However, since the ocean tidal and well data have temporal measurement uncertainties at least on the order of one hour, the time-lag estimates are equally uncertain and could be a reason for the positive values.

6.3 Specific Storage

The storage coefficient S of an aquifer is defined as the volume of water the aquifer releases from storage per unit surface area per unit decline in head (dimensionless). Assuming a constant fluid compressibility, the storage coefficient is a function of four variables: the specific weight of the water (γ_w), the porosity of the rock (θ), the compressibility of the aquifer, and the thickness of the aquifer (Δz). For known salinity and temperature conditions, the specific weight of water can be calculated with relative precision. The compressibility of the aquifer is expressed by the barometric efficiency, as shown in equation 6. That leaves two remaining unknowns, aquifer thickness and porosity, to be determined before a storage coefficient can be estimated.

In a homogeneous, isotropic medium, the determination of aquifer thickness is a straightforward process, but the heterogeneity of the FAS leads to some uncertainty in this parameter. Aquifers of the FAS are characterized by one or more relatively discrete permeable zones separated by semi-confining, or simply less permeable rock. At what point should the top of an aquifer be defined; the first occurrence of a highly permeable zone, or the first occurrence of non-confining material? The same question can be posed for determination of the base of the aquifer. How these questions are answered largely depends on the objective of the individual making the determination, and the data available with which to make it.

The thickness of the Lower Floridan in well BF-1 provides a good example of the uncertainties involved. Between depths of 1,074 and 1,170 feet below land surface, the well penetrates alternating layers of crystalline

dolomite and limestone, but no sign of permeability occurred until a depth of 2,124. Between 2,124 and 2,170, the drill bit dropped abruptly through at least two cavities up to two feet in diameter. The caliper log also indicated sudden large increases in borehole size at three separate intervals (2,124 - 2,126; 2,136 -2,141; 2,146 - 2,147 ft) indicating cavities or fractures.

What is the thickness of the aquifer? An argument could be made that the effective aquifer thickness is simply the sum of the fractured or solutioned intervals, which would exhibit permeability orders of magnitude larger than the intervening limestone units. On the other hand, there is no evidence to suggest the higher permeability intervals are hydraulically isolated from each other. In this report we will utilize the aquifer thickness values defined by [Lukasiewicz, 2003] and [Lukasiewicz, 2001]. It is important to recognize, however, that there is a certain amount of subjectivity in the determination of this variable.

There is also uncertainty in the estimation of aquifer porosity. Porosity can be measured directly in the laboratory using rock core samples, but core recovery is expensive and technically difficult in the FAS. Laboratory measurements also can not account for larger scale secondary porosity due to fracturing or dissolution cavities in the rock. In karstic rock, porosity is more generally estimated in situ, by indirect measurement techniques. Median porosity within each hydrostratigraphic unit was estimated for this project from neutron porosity logs. Neutron logs measure hydrogen content within the formation. Assuming that all of the measured hydrogen is tied up in interstitial water, porosity can be calculated. The presence of hydrogen as a mineral constituent (e.g. in clay), will bias this estimate. The presence of saturated, but disconnected pore space, not contributing to the effective porosity of the rock, will also bias porosity from neutron logs. Both of these biases tend toward over-estimation of porosity.

Estimates of specific storage and storage coefficient for each of the Floridan Aquifer zones were computed with the use of equations 6 and 7, results are shown in table 14. The resultant values of S are used to compute parameters p, q and C_e of equation 3. The value of water compressibility for all calculations is β=4.4E-10 (m^2/N).

6.4 Aquifer Diffusivity

Diffusivity D, is the ratio of transmissivity to storage coefficient [Length^2/time]. This parameter is not frequently used by hydrogeologists, but it has important implications for regional aquifer evaluation, because it controls the speed with which the effect of any stress is propagated through the aquifer.

Well	Δz (ft)	γ_w (N/m^3)	B_e	θ	S_s (/m)	S_s (/ft)	S
PBF-3	202	9,818	0.71	0.37	2.25E-6	6.86E-7	1.39E-4
PBF-4	150	9,820	0.72	0.30	1.80E-6	5.49E-7	8.23E-5
PBF-5	150	10,008	0.67	0.25	1.64E-6	5.01E-7	7.51E-5
BF-1	46	10,017	0.59	0.22	1.64E-6	5.01E-7	2.30E-5

Table 14: Estimates of Specific Storage S_s and Storage Coefficient S.

Diffusivity can be calculated from the results of multi-well aquifer performance testing (APT).

This section compares results of diffusivity estimated from aquifer performance tests with analytical results from previous sections at each of the well sites. Analytical diffusivity values are determined by the method of Van der Kamp (equation 4), Ferris (equation 5), and Li & Jiao (equation 3). Parameter values for inland well distance, aquifer barometric efficiency and loading efficiency, are tabulated in table 15.

Well	x_o (ft)	B_e	L_e
PBF-3	24,335	0.71	0.29
PBF-4	24,335	0.72	0.28
PBF-5	24,335	0.67	0.33
BF-1	24,226	0.59	0.41

Table 15: Inland well distance and aquifer loading parameters.

6.4.1 APT Diffusivity

Diffusivity values were estimated from aquifer performance tests conducted at the upper and middle Floridan Aquifer wells PBF-3 and PBF-4. The transmissivity and storage coefficient values were calculated by [Lukasiewicz, 2001] using the [Hantush, 1956] analytical solution for pumping tests in leaky aquifers. There are limitations to such analytical solutions. One that is always a concern in aquifers distinguished by secondary porosity and preferential flow pathways, is the requirement that groundwater flow in the aquifer be horizontal and directed radially toward the well. This assumption is generally valid for values of the function $(r/B) < 0.1$. Since [Lukasiewicz, 2001] reports (r/B) values of 0.247 and 0.1 for PBF-3 and PBF-4 respectively, it is probable that some element of vertical flow is present during testing.

It is then useful to have an independent check on the analytical solution. [Streltsova, 1988] offers an approximation of diffusivity based solely on the time required for pumping stress to be realized at an observation well located a distance r from the stress ($r = 2\sqrt{Dt}$). [Lukasiewicz, 2001] records that drawdown began within 60 seconds (PBF-3) and 9 seconds (PBF-4) of initiation of pumping at a well 260 feet away. Diffusivity estimates derived from APT results are summarized in table 16.

Well	T(ft^2/day)	S	D_1 (ft^2/s)	D_2 (ft^2/s)
PBF-3	34,300	0.0036	110	272
PBF-4	198,500	0.00085	2,703	1,878

Table 16: Diffusivity estimated from aquifer performance tests. D_1 D_2

6.4.2 Ferris Diffusivity

The method of Ferris (equation 5) assumes a vertical aquifer outcropping at the coastal boundary, results of this formulation are presented in Table 17.

Mode	PBF-3 (ft^2/s)	PBF-4 (ft^2/s)	PBF-5 (ft^2/s)	BF-1 (ft^2/s)
O_1	4,380	6,239	7,643	7,384
N_2	4,060	7,509	9,796	9,525
M_2	4,073	7,706	9,948	9,870

Table 17: Aquifer diffusivity with method of Ferris.

Diffusivity estimated by the method of Ferris is approximately 37 times greater than the PBF-3 measurement, and roughly 3 times greater than the PBF-4 data.

6.4.3 Van der Kamp Diffusivity

The method of Van der Kamp assumes a confined aquifer extending infinitely under the ocean, and is evaluated according to equation 4. Table 18 lists estimates of aquifer diffusivity based on the coupling coefficients of table 12 applied to equation 4.

Mode	PBF-3 (ft^2/s)	PBF-4 (ft^2/s)	PBF-5 (ft^2/s)	BF-1 (ft^2/s)
O_1	472,236	646,666	589,106	6,912,874
N_2	26,560	305,938	711,968	178,479
M_2	25,973	324,233	699,121	195,049

Table 18: Aquifer diffusivity with method of Van der Kamp.

Results from the alternative formulation employing the phase values of table 9 in equation 4 are shown in table 19.

Mode	PBF-3 (ft^2/s)	PBF-4 (ft^2/s)	PBF-5 (ft^2/s)
O_1	91,931	2,383,354	987,539,321
N_2	259,358	3,230,664	887,922
M_2	438,043	1,174,258	675,322

Table 19: Aquifer diffusivity with method of Van der Kamp.

These estimates are clearly not compatible with the measured results, therefore the aquifer conditions consistent with the Van der Kamp formulation are assumed not to reflect that of the S.E. Florida coast.

6.4.4 Li & Jiao Diffusivity

If the aquifer geometry corresponds to that shown in figure 11 with an unconfined surficial aquifer leaking into a semi-confined aquifer which extends under, and eventually outcrops into the ocean, the method of Li & Jiao can be used. As noted in section 3.1.1, equation 3 applies to the inland portion of the geometry. It should be noted that computation of C_e in equation 3 depends on the distance L which the semi-confined aquifer extends under the ocean to the outcropping, by a factor $f \approx e^{-pL}e^{-iL}$. Estimates of L for the wells range from 45,000 to 133,000 ft, therefore, the terms which contribute to C_e for the submerged aquifer length are essentially zero, corresponding to a semi-infinite lateral extent of the semi-confined aquifer.

The leakance parameters p and q of equation 3 require specification of a vertical leakance L_S (/day). In Merritt's analysis the range of leakance values for the intermediate confining unit span the interval 1E-6 to 2E-5 [Merritt, 2004]. Results of equation 3 using the mean value of this range (L_S = 1.05E-5 (/day)), are listed in table 20.

The majority of values computed by the Li & Jiao method are close to

Mode	PBF-3 (ft^2/s)	PBF-4 (ft^2/s)	PBF-5 (ft^2/s)	BF-1 (ft^2/s)
O_1	374,991	3,829,778	2,279,153	208,996
N_2	27,263	285,435	644,563	144,630
M_2	26,660	302,877	637,945	157,275

Table 20: Aquifer diffusivity with method of Li & Jiao, $L_S = 1.05\text{E-}5$ (/day).

the values of Van der Kamp, and are not consistent with APT estimates. That these values are close to the Van der Kamp results indicates that a fundamental mismatch between the actual geophysical configuration of the FAS in the LEC and that of the Li & Jiao geometry.

7 Conclusion

Groundwater levels respond to mechanical stresses such as barometric pressure or changes in ocean tides. This paper has explored the use of spectral analysis and linear systems modeling for evaluating those responses, and applying them to characterization of the Floridan Aquifer System on the southeast coast of Florida. Three objectives were pursued:

1. Characterization of aquifer hydraulic properties in the absence of traditional field testing.
2. Provision of independent information on off-shore (ocean-to-aquifer) boundary conditions to guide model calibration.
3. Evaluation of spectral analysis methods, routinely used in signal processing applications to hydrogeologic investigation.

These objectives met with varying degrees of success.

Analysis focused on 4 coastal Floridan Aquifer wells, three in Palm Beach County, and one in Broward County. All of these wells were shown to be strongly influenced by ocean tidal forcing. This would imply that these wells should be good candidates for application of tidal forcing models for calculation of their hydraulic properties. Three analytical models based on distinct geological formation criteria (Ferris, Van der Kamp, and Li & Jiao) were applied to estimate hydraulic properties based on tidal forcing.

A primary physical variable of the analytical models is the ratio between the strength of the ocean tidal pressure forcing and the strength of the well response to the tidal forcing. These variables were termed coupling coefficients, and were quantified by power spectral analysis. An alternative formulation based on the time lag (phase-shift) between the ocean forcing and well response can be applied for each model. This approach has the benefit of providing an estimate of diffusivity independent of the barometric efficiency, however, it requires temporal synchronization between the ocean tide and groundwater level measurements. Nonetheless, the phase formulation was evaluated based on phase-shifts computed directly from cross-spectral densities of the tidal and aquifer data. Time delays computed from these values were consistent with observations of the timeseries, within the uncertainty of the temporal accuracy.

Application of coupling coefficients for all three models produced estimates of diffusivity that were inconsistent with APT values measured at PBF-3, 4 and BF-1; at least an order of magnitude higher than should

reasonably be expected. Likewise, the phase-shift formulation produced estimates that were not reasonable. The reasons for this failure are not entirely clear. One possible interpretation is that none of the three hydrogeological analytical models corresponds well with the field conditions found at the well sites.

Even though assessment of effective hydraulic properties of the FAS could not be obtained from the ocean tidal forcing analysis, there is still useful information to be gained from the analysis that can provide guidance to numerical modeling efforts. Of the three analytical models evaluated, our physical conceptualization of the FAS most closely resembles the Li & Jiao model; a dual system, where ocean and aquifer interact directly at the offshore outcrop of the aquifer, and indirectly (through pressure loading) between the outcrop and the shore. Most numerical models in the FAS try to explicitly simulate the direct interaction as a boundary condition, but ignore the indirect interaction. The results of the current analysis indicate that along the east coast, at short timescales, to ignore the indirect effect of ocean tidal forcing is to ignore the single largest stress on the aquifer. This is particularly true in the lower Floridan, which is devoid of anthropogenic activity. Indeed, it is demonstrated that at the tidal frequencies of O_1, N_2 and M_2, the aquifer well variance is 95.8% to 99.9% driven by the tidal forcing. The ocean tidal forcing offers an opportunity to improve model calibration in the otherwise un-stressed portions of the FAS.

Another useful finding of the analysis concerns calculation of barometric efficiency, a critical component for accurate estimates of both storage coefficient and tidal efficiency. It was found that strong tidal coupling can overwhelm barometric response at short timescales where barometric forcing is assumed to dominate. This invalidates assumptions inherent in Clark's method for estimating barometric efficiency, corrupting estimates from this usually robust methodology.

To address this concern, a linear systems spectral analysis attempted to estimate the barometric efficiency from ratio's of tidal and aquifer piezometric variances. The results were unsatisfactory. The invalid results were attributed to non-linear coupling between the barometric pressure atmospheric tide component S_1 and the well response.

These barometric efficiency issues suggested that we should estimate B_e over timescales where ocean tidal forcing is not observed. Barometric efficiency estimates were revised accordingly, but the variation in barometric efficiency did not change the inconsistent results of the Ferris, Van der Kamp, and Li & Jiao models. It is reasonable to conclude that none of these models is an adequate physical representation of the FAS in the east coast region.

The final objective of this report was the evaluation of various spectral analysis methods for application to hydrogeologic investigation. Despite the obvious problems with this particular geophysical analysis, it is believed the spectral analysis methodology holds significant promise for hydrogeologic inquiry. Among these positive findings are:

1. Linear system modeling with coherence allows isolation of spectral components of aquifer well response from tidal forcing which do not couple atmospheric pressure forcing.
2. The coherence method has the advantage that data filtering and detrending is not required.
3. Tidal modes O_1, N_2 and M_2 can be used to determine ocean tidal to aquifer coupling coefficients, provided that M_2 SNR is large enough, and that linear system assumptions are valid.

References

[Apel, 1987] Apel, J. R., 1987. Principles of Ocean Physics, Academic Press Inc., ISBN 012058865X

[Bendat, 1986] Bendat, J. S., Piersol, A. G., 1986. Random Data Analysis and Measurement Procedures, 2nd Ed., John Wiley & Sons, ISBN 0471040002

[Brassington, 1998] Brassington R., 1998. Field Hydrogeology 2nd Ed., John Wiley & Sons, p. 102, ISBN 0471973475

[Chapman, 1970] Chapman, S., 1970. Atmospheric Tides, Gordon & Breach Science Publishers, NY, ISBN 0677618107

[Davis, 1993] Davis, D. R., Rasmussen, T., C., 1993. A Comparison of Linear Regression With Clark's Method for Estimating Barometric Efficiency of Confined Aquifers, Water Resources Research, 29(6), p. 1849-54

[Ferris, 1951] Ferris, J. G., 1951. Cyclic fluctuations of water level as a basis for determining aquifer transmissibility. International Geodesy Geophysics Union, Assoc. Sci. Hydrology Gen. Assembly, Brussels, 2, p. 148-155; Reproduced as: U.S. Geological Survey, Water Resources Division, Ground Water Branch, Washington D.C. Contribution No. 1, April 1952.

[Hantush, 1956] Hantush, M.S., 1956. Analysis of Data from Pumping Tests in Leaky Aquifers. American Geophysical Union Transactions. Vol. 37, No. 6.

[Jacob, 1950] Jacob, C. E., 1950. Flow of groundwater, in Engineering Hydraulics, editor H. Rouse, p. 321-86 John Wiley & Sons, New York, ISBN 047174283X

[Jacob, 1940] Jacob, C. E., 1940. The flow of water in an elastic artesian aquifer, Eos Trans., AGU, 21, p. 574-86

[Li and Jiao, 2001] Li, H, and Jiao, J. J., 2001. Tide-induced groundwater fluctuation in a coastal leaky confined aquifer system extending under the sea, Water Resources Research, 37(5), p. 1165-71

[Lukasiewicz, 2001] Lukasiewicz, John, Richard Nevulis, Milton Switanek, and Robert Verrastro, 2001. Final Report: Floridan Aquifer System Test Well Program at Lake Lytal Park, West Palm Beach, Florida. SFWMD Technical Publication WS-5. September, 2001.

[Lukasiewicz, 2003] Lukasiewicz, John, 2003. Floridan Aquifer System Test Well Program C-13 Canal, Oakland Park, Florida. SFWMD Technical Publication WS-16. April, 2003.

[Merritt, 2004] Merritt, M. L., 2004. Estimating Hydraulic Properties of the Floridan Aquifer System by Analysis of Earth-Tide, Ocean-Tide, and Barometric Effects, Collier and Hendry Counties, Florida, U.S. Geological Survey, Water-Resources Investigations Report 03-4267, Tallahassee, Florida.

[NOAA LKWF1, 2006] NDBC C-MAN Station LKWF1 - Lake Worth, FL `http://www.ndbc.noaa.gov/station_page.php?station=lkwf1` Location: 26°36'42" N 80°02'00" W

[NOAA FWYF1, 2006] NDBC C-MAN Station FWYF1 - Fowey Rocks, FL `http://www.ndbc.noaa.gov/station_page.php?station=fwyf1` Location: 25°35'25" N 80°05'48" W

[Rasmussen, 1997] Rasmussen, T., C., Crawford, L., A., 1997. Identifying and Removing Barometric Pressure Effects in Confined and Unconfined Aquifers, Ground Water, 35(3), p. 502-11

[Ritzi, 1991] Ritzi, R. W., Sorooshian, S., Hseih, P. A., 1991. The Estimation of Fluid Flow Properties From the Response of Water Levels in Wells to the Combined Atmospheric and Earth Tide Forces, Water Resources Research, 27(5), p. 883-93

[Rojstaczer, 1988a] Rojstaczer, S., 1988. Intermediate period response of water levels in well to crustal strain: sensitivy and noise level, Journal of Geophysical Research, 93(11), p. 13,619-34

[Rojstaczer, 1988b] Rojstaczer, S., 1988. Determination of Fluid Flow Properties From the Response of Water Levels in Wells to Atmospheric Loading, Water Resources Research, 24(11), p. 1927-38

[Sophocleous, 2004] Sophocleous, M., et. al. Can precipitation loading be detected at 300 meter depth or greater? Kansas Geological Survey, Open File Report 2004-46, University of Kansas, Lawerence, KS.

[Streltsova, 1988] Streltsova, Tatiana D., 1988. Well Testing in Heterogeneous Formations. An Exxon Monograph. John Wiley & Sons.

[Van der Kamp, 1969] Van der Kamp, G. S., Carr, P. A., 1969. Determining Aquifer Characteristics by the Tidal Method, Water Resources Research, 5(5), p. 1023-31

[Van der Kamp, 1972] Van der Kamp, G., 1972. Tidal fluctuations in a confined aquifer extending under the sea, International Geological Congress, 24(11), p. 101-6